Macromolecules
Cite This: Macromolecules XXXX, XXX, XXX−XXX
Article
pubs.acs.org/Macromolecules

Glass Transition and Self-Diffusion of Unentangled Polymer Melts Nanoconfined by Different Interfaces

Reika Katsumata,[†] Austin R. Dulaney,[†] Chae Bin Kim,[†] and Christopher J. Ellison*[,†,‡]

[†]McKetta Department of Chemical Engineering, The University of Texas at Austin, Austin, Texas 78712, United States
[‡]Department of Chemical Engineering and Materials Science, The University of Minnesota - Twin Cities, Minneapolis, Minnesota 55455, United States

Supporting Information

ABSTRACT: In nanoconfined thin films, numerous studies have revealed the thickness dependencies of different thermophysical properties, including the glass transition temperature (T_g) and self-diffusion coefficient (D). While quantitative relationships between these properties are well-known for bulk polymers, analogous relationships for nanoconfined polymers are still not clear. Herein, T_g−D relationships are studied under nanoconfinement using spectroscopic ellipsometry for measuring T_g and fluorescence recovery after photobleaching for measuring D. Poly(isobutyl methacrylate) (PiBMA) was selected as a model unentangled polymer, and it was nanoconfined to 14−300 nm thick films. Multilayered geometries incorporating PiBMA were constructed to systematically study the influence of free surfaces (i.e., polymer surfaces exposed directly to air, also called uncapped) and surfaces that were in contact with a secondary polymer (also called capped). This multilayer approach additionally allowed investigation of both relatively weak and strong interactions between the polymer and substrate, depending on the existence of hydrogen bonding. The T_g−D relationship observed in nanoconfined thin films deviated from that in the bulk state (e.g., as described by Williams−Landel−Ferry and Stokes−Einstein, or similar relationships). A model was employed that considered the effects of molecular friction between the different confining interfaces and PiBMA, and it successfully described the deviation from bulk behavior.

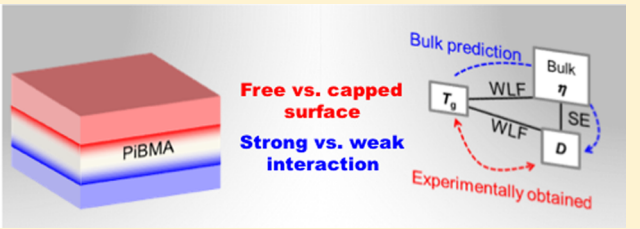

INTRODUCTION

Nanoconfined polymer films often exhibit different physical properties compared to bulk, including glass transition temperature (T_g),[1−8] viscosity (η),[9−13] modulus,[14−16] and self-diffusion coefficient (D).[17−19] However, most studies have revealed how these properties change with film thickness separately, and properties are rarely studied collectively in identical nanoconfined systems. Nonetheless, one overarching theme has emerged where the increasing interfacial area to volume ratio with decreasing film thickness can result in interfacial effects making significant contributions to many thin film properties. As a specific example, previous research has shown that the T_g of polystyrene (PS) thin films supported on SiO_x substrates (e.g., Si wafers with native oxide) decreases as film thickness decreases below about 50 nm;[1,2,4,5,20] this decrease in T_g has been attributed to higher segmental mobility near the free surface that dominates the overall film T_g and the presence of a relatively weak interaction between PS segments and the SiO_x substrate.[21−24] On the contrary, a strong interaction between poly(2-vinylpyridine) and SiO_x substrates increases the overall film T_g by tens of degrees as the film thickness decreases, apparently dominating over the effect expected at the free surface.

There are many other examples reinforcing this theme, yet it remains unclear[20,25] how interfacial effects may distort established bulk relationships between different physical properties, such as T_g and D, in nanoconfined systems.[20,26] Prior to discussing nanoconfinement effects, correlations between the thermophysical properties of bulk polymers are summarized in Figure 1. In terms of dynamic length scale, T_g reflects the cooperative segmental mobility of 10s−100s of repeat units (i.e., short length scale), whereas D and η are related to the large-scale transport of the entire chain (i.e., long length scale). An obvious point of comparison is the bulk T_g−D relationship expressed by the Williams−Landel−Ferry (WLF) equation shown in Figure 1,[27,28] where c_1, c_2, and T_0 are constant while $T_0 = T_g + T_1$ is a reference temperature T_1 degrees higher than T_g.[29] On the other hand, the D−η relationship in bulk follows the Stokes−Einstein (SE) equation: The SE equation describes the correlation between D and η via friction between molecules. From a force balance between the chemical potential gradient and drag force, D can also be expressed as $k_BT/N\zeta$, where k_B is the Boltzmann constant, ζ is friction coefficient between monomers themselves, and N is the degree of polymerization.[30,31] The SE equation is not valid for all conditions, and the deviation from this relationship is known as the "breakdown in the SE relationship". The breakdown of the SE relationship is often

Received: March 5, 2018
Revised: August 7, 2018

DOI: 10.1021/acs.macromol.8b00475
Macromolecules XXXX, XXX, XXX−XXX

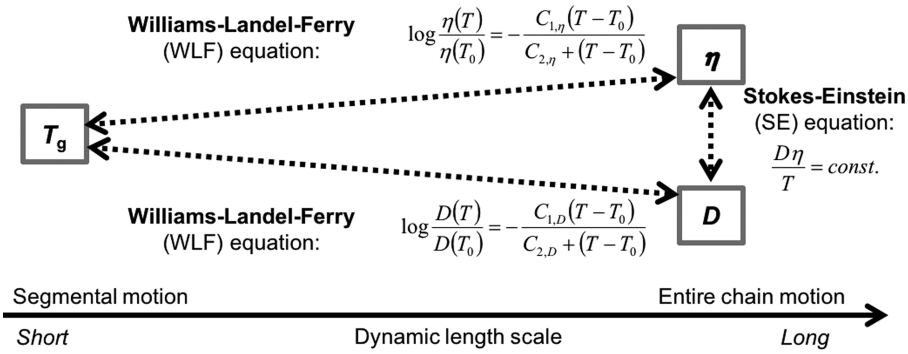

Figure 1. Schematic illustration of the bulk relationship between T_g (glass transition temperature), η (viscosity), and the self-diffusion coefficient (D), where T is the experimental absolute temperature, T_0 is a reference temperature, and C_1 and C_2 are constants.

explained by a dynamic heterogeneity argument.[32] As temperature decreases toward T_g, the polymer becomes more spatially heterogeneous with domains that are estimated to be ~3 nm with the time scales of the "slow" and "fast" regions differing by a range of 1−5 orders of magnitude.[32−37] In this study, it is hypothesized that confining interfaces could cause deviations from well-established bulk correlations based on the WLF and SE equations and that these deviations could be a function of the interfacial interactions.

Given the thickness trend for the nanoconfined T_g of PS supported on SiO_x described in a previous paragraph and assuming the bulk relationship described by the WLF equation is valid, an increase in D would be expected with decreasing film thickness. Counterintuitively, the D of nanoconfined PS along both in-plane (parallel to the interfaces)[17] and out-of-plane (perpendicular to the interfaces)[18] has been reported to be reduced relative to bulk values with decreasing PS film thickness. In contrast, faster dewetting,[38] surface self-diffusion,[39] and leveling of PS thin films on SiO_x substrates have also been reported,[40] corresponding to a higher D than that of bulk. Recently, experimental attempts were made to measure T_g and D in the same thin film systems, suggesting the T_g−D relationship does not follow the bulk relationship and is strongly influenced by interfaces.[41−43] For example, Geng et al. measured T_g, D, and η of poly(isobutyl methacrylate) (PiBMA) supported on a SiO_x substrate and observed that both the T_g and D were independent of the film thickness, while η decreased with decreasing film thickness.[41] These nanoconfinement effects were explained using a three-layer model that accounted for interfacial interactions near the free surface (air) and the SiO_x substrate.[41] Also, Zhang and Fakhraai measured surface diffusion of 12−400 nm thick *N*,*N*′-bis(3-methylphenyl)-*N*,*N*′-diphenylbenzidine (TPD) thin films and reported invariant surface diffusion with film thickness although T_g decreased with reductions in the film thickness.[42] It is clear that interactions between polymer films and neighboring substrates can play a crucial role in the dynamics of polymers under nanoconfinement and, by extension, to defining the T_g−D relationship for nanoconfined systems.[8,41,44−47]

As summarized in recent reviews,[45,48,49] numerous theoretical approaches have been applied to elucidate the T_g−D relationship under nanoconfinement.[29,50−57] For example, early work using the lattice model predicted both a reduced and enhanced D near an impenetrable wall, depending on whether there were attractive and repulsive interactions between the polymer segments and the wall.[29] Other theoretical approaches have also been implemented for similar studies including mode coupling,[51,52,53] free volume hole diffusion,[57] random first-order transition,[56] and the limited mobility lattice models/theories.[54] Although these studies have reached a consensus that more heterogeneous dynamics emerge both with decreasing temperature or as interfaces are approached, a full picture that includes focused experimental measurements has yet to emerge.[43] One specific challenge is translating realistic experimental conditions, such as surface energies, mechanical properties, etc., of the substrate−polymer pairs, into useful parameters that may serve as input to theories/models. To leverage the findings of these important theoretical works, an experimental investigation that systematically studies interfacial effects on both T_g and D in a convenient polymer system is strongly desired.

To provide additional clarity (and to perhaps explain the inconsistentcies between D and T_g for the thin film experiments mentioned above), a study of the T_g−D relationship in a model nanoconfined system was pursued; in this study, a model unentangled PiBMA system was selected, and it was studied in multilayer thin film geometries that additionally afford tailorable interfacial interactions at both nanoconfining interfaces (top and bottom). Furthermore, a low molecular polymer system is examined to exclude the effects of entanglements whose density can change with film thickness and nanopore size,[19,26,58,59] with obvious consequences on whole polymer chain mobility.[31] In the multilayered system described here, the T_g−D relationship was first experimentally studied by ellipsometry to measure T_g and then by fluorescence recovery after patterned photobleaching (FRAPP) to measure D. Then the experimentally obtained T_g−D relationship was compared with that of bulk using the WLF and SE relationships, and decoupling from bulk behavior was explained based on a friction analysis that assigned characteristic molecular friction behavior between polymer segments and differing adjoining interfaces.

EXPERIMENTAL SECTION

Material Synthesis. All reagents were purchased from Sigma-Aldrich, Acros Organics, or Fisher Scientific and used as received unless otherwise noted. A nearly monodisperse PiBMA below its entanglement molecular weight (~28 kDa)[60] was synthesized by activators regenerated by electron transfer atom transfer radical polymerization (ARGET ATRP) as previously reported.[41] For the FRAPP measurements, a fluorescence probe, nitrobenzofurazan (NBD), was covalently attached to PiBMA as an end-group using a NBD-labeled initiator. Our previous study showed that end-chain-labeled and middle-chain-labeled PiBMA−NBD exhibited the same D

DOI: 10.1021/acs.macromol.8b00475
Macromolecules XXXX, XXX, XXX−XXX

within 95% confidence of error.[61] While the details of the synthesis can be found in previous work,[41] the NBD−PiBMA employed here incorporated NBD via covalent attachment to an ethyl α-bromoisobutyrate (EBIB) initiator following a published procedure;[61] unlabeled PiBMA was synthesized with EBIB under identical conditions as a control. The ratio of monomer (iBMA):initiator (EBIB or NBD−EBIB):catalyst (copper(II) bromide):ligand (tris[2-(dimethylamino)ethylamine):reducing agent (tin(II) 2-ethylhexanoate) was 50:1:0.02:0.2:0.1. The reaction was conducted in anisole (0.5 g/mL to monomer) for 10 h at 80 °C.

Material Characterization. Molecular weight was measured using size exclusion chromatography (SEC) using a Viscotek Max VE 2001 equipped with a Viscotek Model 270 dual viscometer/light scattering detector and a Viscotek VE 3580 refractive index detector. Two Viscotek I-series mixed-bed low-molecular-weight columns were used with tetrahydrofuran (THF) eluent at a flow rate of 1 mL/min. The number-average molecular weight (M_n) of the synthesized PiBMA-NBD was determined to be M_n = 12.2 kDa, with $Đ$ = 1.2, and that of the unlabeled PiBMA was M_n = 10.0 kDa, with $Đ$ = 1.1. Complete removal of the unattached NBD was confirmed by an inline fluorescence detector (Jasco FP-2020; $\lambda_{excitation}$ = 465 nm, $\lambda_{emission}$ = 520 nm) attached to the SEC showing no small-molecule fluorescence peak from unattached NBD. The NBD content in the PiBMA-NBD was determined as 1.27 wt % with a Thermo Scientific Evolution 220 UV−vis spectrophotometer, using 0.001−0.025 mmol NBD/THF solution for calibration.

Preparation of Multilayer Films. Prior to spin-coating, substrates were cleaned in a solution of 10:10:80 wt % potassium hydroxide:deionized water:ethanol solution and rinsed with deionized water and THF at least three times. All polymer solutions for spin-coating were filtered through 0.2 μm pore-size Teflon filters to remove dust particles. PiBMA films were spin-coated from *n*-butanol (1.0−8.0 wt %, 1800−3800 rpm) onto polished quartz substrates (for FRAPP measurements) or Si wafers (for T_g measurement to gain reflectance) with 1.5−2.0 nm thick native oxide. These substrates are regarded to be similar in terms of the interactions with PiBMA because they exhibit similar hydroxyl densities when properly pretreated (~5−7 hydroxyls/nm^2).[61,62] Polycyclohexylethylene (PCHE) layers (105 ± 5 nm) were also spin-coated onto Si wafers from 2 wt % toluene solutions at 1800 rpm. The films were annealed for 20 min under vacuum at 120 °C ($T_{g,PiBMA}$ + 62 °C) for PiBMA and 150 °C ($T_{g,PCHE}$ + 7 °C) for PCHE to remove residual stress and solvent. The PCHE capping layers were prepared by floating the spin-coated PCHE film on cold "(< 5 °C) water, while the PiBMA on top of the PCHE was prepared by sequential spin-coating using orthogonal solvents. The final multilayered samples were dried at 35 °C overnight and then annealed at 150 °C for 10 min under vacuum to be sure they were completely free of residual solvent and water.

Thin Film T_g Measurements. To evaluate the film T_g, PiBMA film thicknesses were measured as a function of temperature with a cooling rate of 2 °C/min using a spectroscopic ellipsometer (J.A. Woollam M-2000D) equipped with an Instec mK 1000 temperature controller and HCS 402 hot stage connected to a liquid nitrogen pump as described in previous work.[41] The sample chamber with quartz windows was purged with argon during the measurement to avoid water condensation. The T_g of the films were determined by fitting the data to the following hyperbolic tangent type function:[4]

$$h(T) = w\left(\frac{M-G}{2}\right)\ln\left\{\cosh\left(\frac{T-T_g}{w}\right)\right\} + (T-T_g)\left(\frac{M+G}{2}\right) + c \quad (1)$$

where c is the value of the film thickness at $T = T_g$ and w is the width of the transition between the rubbery and glassy states. In this study, the value of w was restricted to be smaller than 35 °C considering the temperature range of the T_g measurement. M and G correspond to the thermal coefficients of expansion of the rubbery and glassy state, respectively. To decrease the number of the fitting parameters, the thicknesses of the PCHE and SiO_x layers were measured at room temperature and used as a constant value during the cooling, similar to a previous study.[61] Although the thickness of these layers changes with temperature, there is no thermal transition in the temperature range of the measurement. Thus, this assumption does not affect the transition temperature of the PiBMA. The validity of this fitting method can be confirmed by the fact that the T_g of thick (>100 nm) films matches with the bulk value regardless of the confining interfaces.

FRAPP Measurements. For patterned photobleaching, a photomask with a 20 μm pitch size (Edmund Optics) was placed on the top of the films with a 360 nm long pass filter to avoid undesired photochemical reactions. The sample was photobleached using a broadband (300−700 nm) light source (Optical Building Blocks Scope Lite 200) with a light intensity of 10 mW/cm^2 for 150 s. The fluorescence intensity profile was observed by an Olympus BX 51 epifluorescence microscope attached to a Photon Technologies Quanta Master 40 fluorometer. The excitation wavelength was 445 nm, and the emission intensity was measured over a range of wavelengths >520 nm. The obtained fluorescence intensity profile[41] as a functional of lateral position, x was fit to a sinusoidal function as shown in eq 2, where $A(t)$ is the amplitude of the sinusoidal intensity, λ is the pitch size, and x_0 and C are fitting parameters.

$$I(x,t) = A(t)\cos\left\{\frac{2\pi(x+x_0)}{\lambda}\right\} + C \quad (2)$$

The specimens were placed on a hot stage at the measurement temperature (106 °C = $T_{g,bulk}$ + 48 °C) for 4 min prior to each measurement to attain equilibrium. Here, $T_{g,bulk}$ corresponds to the bulk T_g of PiBMA as measured by differential scanning calorimetry (DSC; Mettler Toledo DSC-1) with a 10 °C/min heating rate upon second heating. During the FRAPP measurements, argon gas was purged over the sample slowly to avoid fluorescence quenching by oxygen.[63]

RESULTS AND DISCUSSION

Multilayer Film Assemblies. Interfacial effects were systematically investigated using four multilayered geometries with corresponding sample names as shown in Figure 2. The

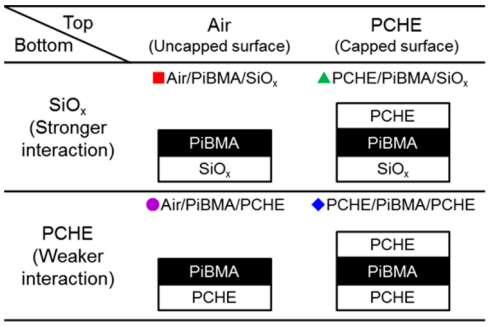

Figure 2. Schematic diagram of film geometries in this study where PiBMA (black) is the layer of interest. PiBMA/SiO_x interfaces exhibit relatively stronger interactions than those of PiBMA/PCHE.

top row in Figure 2 displays the sample geometries with relatively strong interactions between PiBMA and the SiO_x substrate due to hydrogen bonds between the ester groups on PiBMA and the native hydroxyl groups on the SiO_x substrate.[64] The multilayers were prepared by spin-coating with orthogonal solvents or a water floating method; details are available in the Experimental Section. The bottom row in Figure 2 shows the sample arrangements of PiBMA on PCHE substrates, which exhibit relatively weak interactions between PiBMA and the saturated hydrocarbon PCHE layer. Here, PCHE is immiscible with PiBMA[65] and remains in the glassy state during all

DOI: 10.1021/acs.macromol.8b00475
Macromolecules XXXX, XXX, XXX−XXX

measurements due to its higher T_g (144 °C) than the bulk PiBMA (58 °C). To investigate the influence of free surfaces, PCHE was also used as a capping layer, leveraging its excellent transparency to ultraviolet and visible light. For all PiBMA thin films, the T_g and D were characterized by spectroscopic ellipsometry and FRAPP, respectively.

T_g Measurements. To evaluate the film T_g, PiBMA film thicknesses were measured as a function of temperature with a cooling rate of 2 °C/min using a spectroscopic ellipsometer. We note that unlabeled PiBMA was used for T_g measurement because the previous study showed PiBMA−NBD and PiBMA exhibit the same T_g within experimental error.[61] Figure 3a,b shows representative data of the T_g measurements of Air/PiBMA/PCHE with PiBMA thicknesses of (a) 122 nm and (b) 14 nm. The T_g was determined as the transition point where the slope changes by fitting a hyperbolic tangent-type empirical equation (eq 1).[4] As shown in Figure 3a, the T_g of the 122 nm thick film was 58.6 °C, which is close to the bulk value (58 °C) measured by differential scanning calorimetry (DSC) with a heating rate of 10 °C/min during the second heating cycle. This agreement of T_g between ellipsometry (thick film) and DSC (bulk) is consistent with a previous study.[66] In contrast, the T_g of the 14 nm thick film was 46.1 °C, which is ∼12 °C lower than the bulk value. The lower T_g in the nanoconfined Air/PiBMA/PCHE film was attributed to contributions of both the free surface and the weaker interactions between PiBMA and the PCHE substrate, as discussed in detail later.

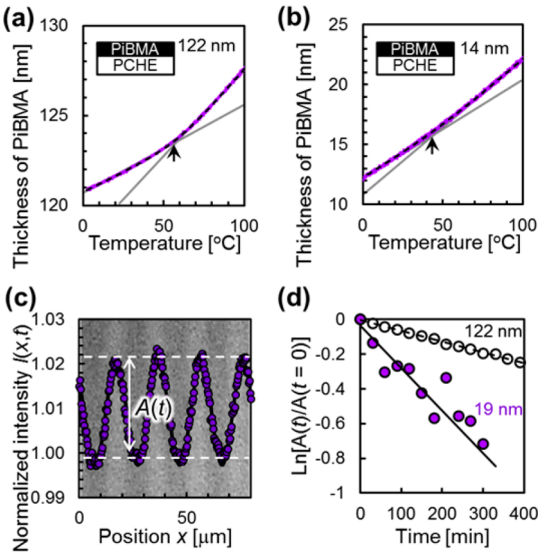

Figure 3. Representative T_g and D data of Air/PiBMA/PCHE samples. (a, b) PiBMA film thickness as a function of temperature prepared on PCHE substrates measured with a cooling rate of 2 °C/min. The solid black lines are a guide to the eye to show slope changes, and dashed lines are the best fit of a hyperbolic tangent-type empirical equation (eq 1).[4] PiBMA thickness at 25 °C was (a) 122 nm and (b) 14 nm. Arrows correspond to T_g = (a) 58.6 °C and (b) 46.1 °C. (c) An example top-down view fluorescence micrograph of a 120 nm thick PiBMA film on a PCHE substrate. The overlaid graph shows normalized intensity as a function of position along the x-axis. (d) Representative data of a FRAPP measurement at 106 °C ($T_{g,bulk}$ + 48 °C). Variation with time of the amplitude of the intensity normalized by the value at t = 0. Open and closed symbols represent a 120 nm thick film and 19 nm thick film, respectively. The solid and dashed lines are the best fit for data using eq 3.

Self-Diffusion Coefficient Measurements. The D of NBD-labeled PiBMA under nanoconfinement was measured by FRAPP at 106 °C ($T_{g,bulk}$ + 48 °C). To avoid self-quenching[67] of NBD, unlabeled PiBMA and labeled PiBMA (PiBMA-NBD) were mixed to limit the NBD content in the polymer film to lower than 0.18 wt %. The D of PiBMA can be obtained by observing how the intensity profile of the photobleached pattern (20 μm in pitch) changes as molecular diffusion occurs, and the detailed procedure is available in the Experimental Section. Figure 3c shows a representative fluorescence micrograph and the corresponding intensity profile along the x-axis. The intensity profile $I(x,t)$ was fit to a sinusoidal function (eq 2),[61] where $A(t)$ is the amplitude of the sinusoidal intensity and λ is the pitch size of the photomask. As self-diffusion of the labeled PiBMA proceeded, the intensity amplitude, $A(t)$, i.e., the difference in intensity between bleached and unbleached regions, also decreased. By fitting $A(t)$ to eq 3, D and the characteristic decay time (τ) can be obtained.

$$A(t) = A(0)\exp\left(-\frac{4\pi^2 Dt}{\lambda^2}\right) = A(0)\exp(-t/\tau) \quad (3)$$

Figure 3d shows the time variation of $A(t)$ for two Air/PiBMA/PCHE films, where the open symbols and closed symbols represent 120 and 19 nm thick films, respectively. The slope of $A(t)$ versus time is proportional to D; the steeper slope of $A(t)$ of the thinner film indicates that the D of Air/PiBMA/PCHE is significantly increased by decreasing the thickness of PiBMA.

Film Thickness Dependence of T_g and D. The trends of T_g and D with PiBMA film thickness were different depending on the multilayered film arrangement. The first row of Figure 4 shows T_g of PiBMA as a function of thickness measured by ellipsometry, and the second row in Figure 4 shows the thickness dependence of D for PiBMA films at 106 °C (= $T_{g,bulk}$ + 48 °C) measured by FRAPP. The dashed lines in the first row of each plot are bulk values of T_g measured by DSC with a heating rate of 10 °C/min during the second heating cycle. The solid lines are obtained by fitting these experimental data to the empirical equation[1] $T_g(h) = T_{g,bulk}\{1 \pm (\alpha/h)^{\delta}\}$, where α and δ are fitting parameters, as listed in Table 1, and h is the thickness of PiBMA. Regardless of the neighboring interfaces, the T_g and D of thick films (>∼100 nm) are in good agreement with $T_{g,bulk}$ and D_{bulk}. Here, D_{bulk} (8.65×10^{-13} cm^2/s) was evaluated based on eq 3 by measuring τ of a 120 nm thick PiBMA film with different pitch sizes, λ from 10.0 to 25.0 μm, and the data are available in the Supporting Information. As was shown in eq 3, the characteristic decay time of the intensity profile for a given D depends on the pitch size of the photomask, λ, and this relationship is commonly used to confirm successful FRAPP measurements.[68] Also, the thickness of irreversibly adsorbed layers of PiBMA on the attractive substrate (SiO_x) was negligible (0.9 ± 0.3 nm) compared to the entire film thickness,[41] indicating PiBMA in the entire film was mobile and measurable by FRAPP.

The different trends of T_g with film thickness in the first row of Figure 4 can be interpreted by considering interfacial effects upon confinement. The nearly unchanged T_g with film thickness for Air/PiBMA/SiO_x can be attributed to counterbalancing of two contributing interfaces: the free surface locally decreasing the T_g and the interaction between PiBMA and SiO_x locally increasing the T_g.[64] In contrast, the T_g of Air/

DOI: 10.1021/acs.macromol.8b00475
Macromolecules XXXX, XXX, XXX−XXX

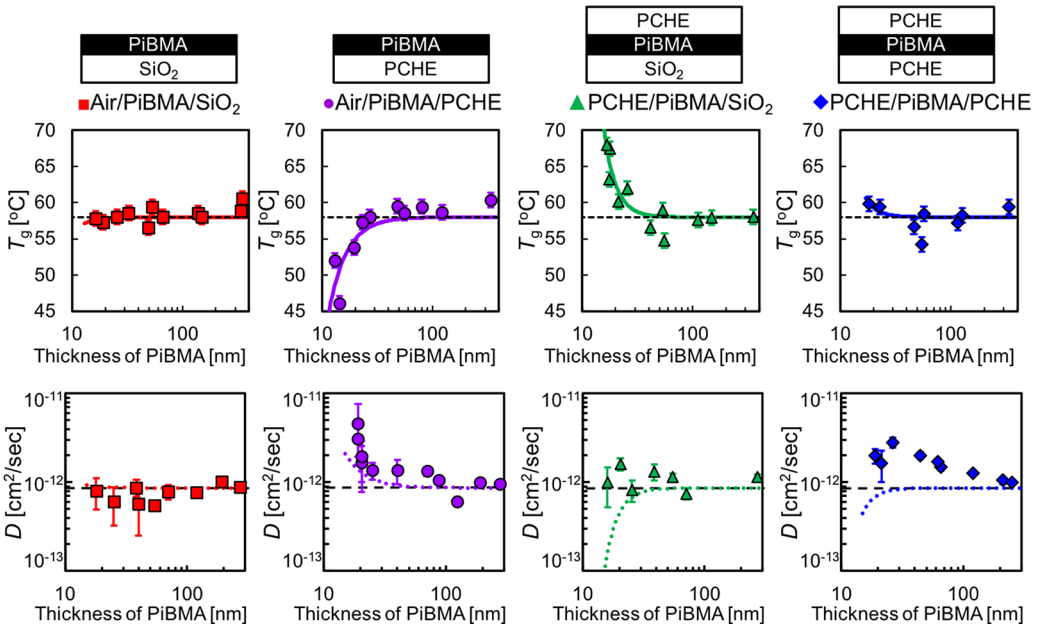

Figure 4. First row: thickness dependence of T_g for PiBMA in Air/PiBMA/SiO_x (red squares), Air/PiBMA/PCHE (purple circles), PCHE/PiBMA/SiO_x (green triangles), and PCHE/PiBMA/PCHE (blue diamonds) measured by ellipsometry. The black dashed lines show T_g of bulk PiBMA (= 58 °C) measured by DSC. The solid lines are fitting curves based on the empirical equation[1] $T_g(h) = T_{g,bulk}\{1 \pm (\alpha/h)^{\delta}\}$. The error bars represent a typical experimental uncertainty of the T_g measurement (± 1 °C). Second row: thickness dependence of D for PiBMA measured by FRAPP at 106 °C ($T_{g,bulk}$ + 48 °C). The dotted lines correspond to D values predicted from T_g values in the first row using eq 5. The black dashed line shows D of bulk PiBMA measured at 106 °C. Error bars represent 95% confidence intervals. The T_g and D data for Air/PiBMA/SiO_x are reproduced from ref 41.

Table 1. Fitting Parameters for the T_g−h Relationship

	Air/PiBMA/SiO_x	Air/PiBMA/PCHE	PCHE/PiBMA/SiO_x	PCHE/PiBMA/PCHE
α [nm]	3.78	6.57	10.7	8.28
δ	3.42	2.65	4.04	4.30

PiBMA/PCHE decreased as the thickness decreased due to relatively weaker interactions between PiBMA and PCHE compared to those between PiBMA and SiO_x. Comparing PCHE/PiBMA/SiO_x (capped) with Air/PiBMA/SiO_x (uncapped), a higher T_g relative to the bulk value was observed in PCHE/PiBMA/SiO_x (capped) thin films (<~30 nm) due to the absence of the free surface and a locally increased T_g near the substrate which dominates. In a symmetric confinement system, the T_g of PCHE/PiBMA/PCHE was in between the T_g of Air/PiBMA/PCHE and the T_g of PCHE/PiBMA/SiO_x.

***D* Prediction from T_g Assuming Validity of Bulk Relationships.** The broken lines in Figure 4 in the second row are D estimated using the measured T_g thickness relationship, $T_g(h)$, shown in the first row of Figure 4. This estimation assumed a bulk relationship between T_g, η, and D based on the WLF and SE equations. To estimate D from η, the SE relationship ($D\eta$ = constant at a constant T) was employed and rewritten as eq 4, where $T_g(h)$ corresponds to solid lines in the first row of Figure 4. The D as a function of $T_g(h)$ was calculated with eq 5, using the zero-shear η of bulk PiBMA as a function of temperature was measured by a shear rheometer. The zero-shear η from T = 85 to 140 °C (raw data are available in the Supporting Information) was fit to the WLF equation as shown in eq 6, where $\eta_0 = 1.61 \times 10^5$ Pa·s, c_1 = 28.8, and c_2 = 160 °C are the fitting parameters and T_0 = 143 °C = $T_{g,bulk}$ + 85 °C. Substituting these WLF parameters (c_1, c_2, and T_0), D as a function of $T_g(h)$ can be calculated as shown in eq 5.

$$\frac{D\{T_g(h)\}}{D_{T_{g,bulk}}} = \frac{\eta_{T_{g,bulk}}}{\eta\{T_g(h)\}} \tag{4}$$

$$D\{T_g(h)\} = D_{T_{g,bulk}}\eta_{T_{g,bulk}} \times \left[\eta_0 \exp\left\{-\frac{c_1(T - T_g + T_0)}{c_2 + (T - T_g + T_0)}\right\}\right]^{-1} \tag{5}$$

$$\eta\{T_g(h)\} = \eta_0 \exp\left\{-\frac{c_1(T - T_g + T_0)}{c_2 + (T - T_g + T_0)}\right\} \tag{6}$$

Experimentally obtained D values deviated from the prediction derived from the bulk SE and WLF relationships depending on the type of neighboring interfaces. For instance, a ~20 nm thick PiBMA film of PCHE/PiBMA/SiO_x exhibited a T_g of ~68 °C ($T_{g,bulk}$ + 10 °C) which is predicted to exhibit a lower expected D than D_{bulk}; the experimentally measured $D_{(PCHE/PiBMA/SiOx)}$ did not follow such a prediction. Because the differences between the bulk prediction and measured D depend on the interfaces between PiBMA and air/substrates in Figure 4, the deviations from the predictions are hypothesized to be due to interfacial effects which significantly influence the self-diffusion of PiBMA.

Friction Model. To take into account interfacial effects on nanoconfined D, a friction analysis was conducted. Friction coefficients can be used to characterize the effect of neighboring confining interfaces on dynamics of polymer melts.[31,69,70] By modifying Lange et al.'s equation[70] for symmetric confinement to asymmetric confinement for some

DOI: 10.1021/acs.macromol.8b00475
Macromolecules XXXX, XXX, XXX−XXX

cases in this study, the effect of the substrates on D of PiBMA can be expressed as eq 7:

$$\frac{D(h)}{D_{bulk}} = \left\{ \frac{h_i}{h}\left(\frac{\zeta_x + \zeta_y}{\zeta_0} - 2 \right) + 1 \right\}^{-1} \quad (7)$$

where h_i is the effective interfacial thickness for all the interfaces to simplify the fitting, and ζ_o, ζ_x and ζ_y correspond to the friction coefficients between PiBMA segments themselves, PiBMA segments and the top interface X and PiBMA segments and the bottom interface Y, respectively, as shown in Figure 5a,

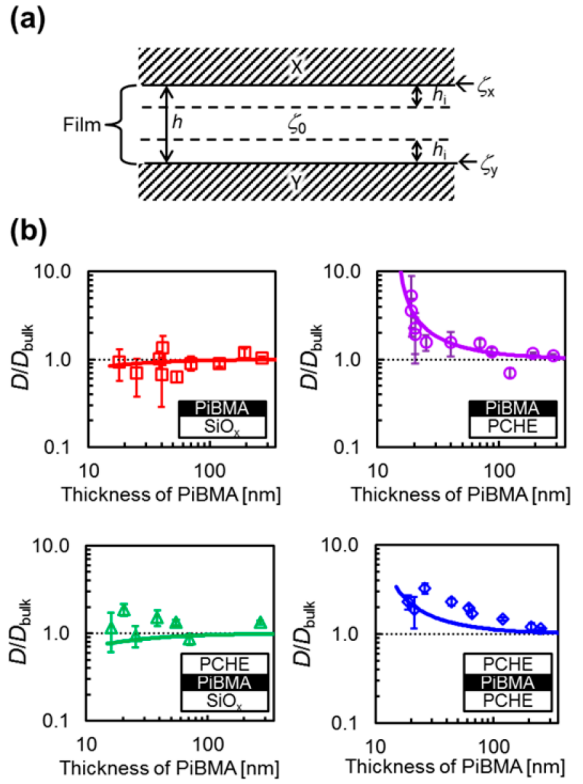

Figure 5. (a) Model used in the friction analysis. (b) D normalized by the bulk value (D_{bulk}) as a function of PiBMA thickness. The solid lines represent fitting using the friction analysis.

respectively. We note that the definition of h_i is still under debate as Lange et al. mentioned[70] and could be different between entangled and unentangled polymers. As a first attempt to apply the friction analysis to this system, h_i is regarded as a fitting parameter. Here, as the ζ_x/ζ_0 or ζ_y/ζ_0 decreases, an increase in the PiBMA melt mobility at or near interface X or Y is expected. The fitting parameters (h_i, $\zeta_{PiBMA/air}$, $\zeta_{PiBMA/PCHE}$, and $\zeta_{PiBMA/SiOx}$) are listed in Table 2, and the detailed procedure of the fitting is described in the Supporting Information.

In Figure 5b, it is noteworthy that the solid line for PCHE/PiBMA/SiO_x using eq 7 described the experimental data well without further adjustable parameters. As previously reported,[70,71] the friction coefficient at a free surface ($\zeta_{PiBMA/air}$) was close to zero, indicating enhanced mobility of PiBMA near the free surface compared to the bulk. Such a small friction coefficient at the free surface is consistent with the enhanced surface diffusion observed by several groups.[39,42,72,73] Also, a higher $\zeta_{PiBMA/SiOx}$ than $\zeta_{PiBMA/PCHE}$ can be attributed to the stronger interaction between PiBMA and SiO_x than that between PiBMA and PCHE. Figure 5b demonstrates that the friction analysis describes the D thickness relationship better than the predictions based on a combination of WLF and the SE equations. This indicates that the deviation from the bulk relationship is due to the fact that the dynamics of PiBMA are convolved with significant contributions from of different interfacial frictions.

Table 2. Fitting Parameters Obtained by the Friction Analysis

h_i [nm]	$\zeta_{PiBMA/air}/\zeta_0$	$\zeta_{PiBMA/PCHE}/\zeta_0$	$\zeta_{PiBMA/SiOx}/\zeta_0$
8.6	9.0×10^{-2}	0.31	2.2

It is worth noting that all reported measurements of T_g and D above are averaged values of different conditions/environments throughout the depth of the film. While it is expected that the method of averaging is different between T_g and D, this difference in averaging cannot alone explain the deviation from the bulk prediction and these friction analyses are still required to understand the T_g–D behavior. The T_g measured by ellipsometry is reported to be a film average of different local T_g's weighted by the difference in thermal expansion coefficient between the liquid and solid states.[74] Therefore, T_g measured by ellipsometry thickness measurements shows a more pronounced deviation from its bulk value compared to that expected from a linear average based on the local density.[74] On the other hand, D measured by FRAPP is an averaged value based on the number fraction of the chains which have a specific *local* D. Considering the Air/PiBMA/PCHE and PCHE/PiBMA/SiO_x systems as examples, Figure 4 shows that the T_g values deviate from their bulk values as the film thickness decreases. But averaging effects may introduce the possibility that the differences in T_g from bulk T_g are more pronounced than a linear average based on the local density. Because the bulk D prediction is based on the T_g values measured by ellipsometry (weighted by the difference in thermal expansion coefficient between the liquid and solid states), it follows that the D prediction could also be more pronounced in terms of its difference from the bulk value due to these averaging effects. Considering the "gap" between the bulk predictions and experimentally obtained D values, an "overestimation" due to T_g and D averaging effects would be expected to *increase* the gap between experimental values and the bulk D prediction in the Air/PiBMA/PCHE system. In contrast, the "gap" would be expected to *decrease* in the PCHE/PiBMA/SiO_x system. Thus, any potential influence of averaging does not affect the deviation from bulk behavior in the same direction, and the friction analysis is still required to explain the D thickness relationship.

The extent to which the T_g–D relationship under nanoconfinement deviates from that of the bulk state varies with film geometries, and this could be explained by differences between the measurement temperature and the thin film T_gs. Although the D was measured at the same temperature for all experiments, 106 °C ($T_{g,bulk}$ + 48 °C) in this study, the T_g of the thin films were different depending on the multilayered arrangement and thickness. For example, in the case of the 20 nm thick PiBMA on SiO_x, the T_g of the film with the capped [uncapped] surface was $T_{g,bulk}$ + 10 °C [~$T_{g,bulk}$], meaning that the temperature gap between the measurement temperature (106 °C) and the film T_g was 38 °C for the capped samples, while it was 48 °C for the uncapped samples. As a result, the

DOI: 10.1021/acs.macromol.8b00475
Macromolecules XXXX, XXX, XXX–XXX

measurement temperature for the capped samples ($T_{g,film}$ + 38 °C) is a relatively lower than the uncapped samples ($T_{g,film}$ + 48 °C). As a comparison, Urakawa and Ediger et al. reported that T_g + ∼40 °C was the temperature where heterogeneous dynamics, i.e., the breakdown of the SE relationship, was observed.[28] Therefore, these different measurement temperatures of D relative to film T_g resulted in the more pronounced effect of heterogeneous dynamics for the capped samples, causing deviation from the SE relationship. Also, considering $D = k_BT/N\zeta$, the temperature dependence of D could be different from the bulk behavior due to the different ζ values associated with different interfacial interactions. In fact, the different temperature dependences from that of the bulk have been reported by Tung et al. in experimental work on nanocomposites[75] and by Torres et al.[50] and Varnik et al.[51] in theoretical work on thin films; further research is needed to fully understand how the temperature dependence of interfacial effects quantitatively contributes to the thickness dependence of D for PiBMA and other model polymer systems.

CONCLUSIONS

In summary, this study examined the relationship between T_g measured by ellipsometry and D measured by FRAPP for unentangled PiBMA under nanoconfinement. The experimentally obtained T_g−D relationship in the nanoconfined state deviated from the bulk relationship established by the WLF and SE equations. To elucidate the mechanism, we employed a model based on friction coefficients between the film and confining interfaces. The friction analysis revealed how three different interfaces altered D distinctly and explained the D thickness behavior. Because the friction coefficient is expected to be a strong function of temperature, further investigation on the temperature dependence of D is needed for a better understanding of nanoconfined self-diffusion.

ASSOCIATED CONTENT

Supporting Information

The Supporting Information is available free of charge on the ACS Publications website at DOI: 10.1021/acs.macromol.8b00475.

Immiscibility of PCHE and PiBMA, bulk D measurement by FRAPP, bulk viscosity measurement, and details of the friction analysis (PDF)

AUTHOR INFORMATION

Corresponding Author

*(C.J.E.) E-mail: cellison@umn.edu.

ORCID

Reika Katsumata: 0000-0003-3119-9385

Chae Bin Kim: 0000-0002-7976-7612

Christopher J. Ellison: 0000-0002-0393-2941

Notes

The authors declare no competing financial interest.

ACKNOWLEDGMENTS

This work is supported by National Science Foundation CAREER Program (Grant DMR-1053293). The authors thank Professor C. Grant Willson for providing use of his facilities and Professor Ophelia K. C. Tsui, Professor David S. Simmons, Dr. Kun Geng, Dr. Kailong Jin, Dr. Heonjoo Ha, Dr. Dustin W. Janes, Dr. Joshua M. Katzenstein, Dr. Sunshine X. Zhou, and Dr. Amanda Jones for helpful discussions. R.K. thanks the Takenaka Scholarship Foundation, Dr. Thomas F. Edgar Endowed Graduate Fellowship in Chemical Engineering, and the Graduate Dean's Prestigious Fellowship Supplement for financial support.

REFERENCES

(1) Keddie, J. L.; Jones, R. A. L.; Cory, R. A. Size-Dependent Depression of the Glass-Transition Temperature in Polymer Films. *EPL* **1994**, *27* (1), 59−64.

(2) Forrest, J. A.; Dalnoki-Veress, K.; Stevens, J. R.; Dutcher, J. R. Effect of Free Surfaces on the Glass Transition Temperature of Thin Polymer Films. *Phys. Rev. Lett.* **1996**, *77* (10), 2002−2005.

(3) Fukao, K.; Miyamoto, Y. Glass Transitions and Dynamics in Thin Polymer Films: Dielectric Relaxation of Thin Films of Polystyrene. *Phys. Rev. E: Stat. Phys., Plasmas, Fluids, Relat. Interdiscip. Top.* **2000**, *61* (2), 1743−1754.

(4) Dalnoki-Veress, K.; Forrest, J. A.; Murray, C.; Gigault, C.; Dutcher, J. R. Molecular Weight Dependence of Reductions in the Glass Transition Temperature of Thin, Freely Standing Polymer Films. *Phys. Rev. E: Stat. Phys., Plasmas, Fluids, Relat. Interdiscip. Top.* **2001**, *63* (3), 031801.

(5) Alcoutlabi, M.; McKenna, G. B. Effects of Confinement on Material Behaviour at the Nanometre Size Scale. *J. Phys.: Condens. Matter* **2005**, *17* (15), R461−R524.

(6) Roth, C. B.; McNerny, K. L.; Jager, W. F.; Torkelson, J. M. Eliminating the Enhanced Mobility at the Free Surface of Polystyrene: Fluorescence Studies of the Glass Transition Temperature in Thin Bilayer Films of Immiscible Polymers. *Macromolecules* **2007**, *40*, 2568−2574.

(7) Yoon, H.; McKenna, G. B. Substrate Effects on Glass Transition and Free Surface Viscoelasticity of Ultrathin Polystyrene Films. *Macromolecules* **2014**, *47* (24), 8808−8818.

(8) Gao, S.; Koh, Y. P.; Simon, S. L. Calorimetric Glass Transition of Single Polystyrene Ultrathin Films. *Macromolecules* **2013**, *46* (2), 562−570.

(9) Hutcheson, S. A.; McKenna, G. B. Comment on "The Properties of Free Polymer Surfaces and Their Influence on The Glass Transition Temperature of Thin Polystyrene Films" by J.S. Sharp, J.H. Teichroeb and J.A. Forrest. *Eur. Phys. J. E: Soft Matter Biol. Phys.* **2007**, *22* (4), 281−286.

(10) Yang, Z.; Fujii, Y.; Lee, F. K.; Lam, C. H.; Tsui, O. K. Glass Transition Dynamics and Surface Layer Mobility in Unentangled Polystyrene Films. *Science* **2010**, *328* (5986), 1676−1679.

(11) McGraw, J. D.; Jago, N. M.; Dalnoki-Veress, K. Capillary Levelling as a Probe of Thin Film Polymer Rheology. *Soft Matter* **2011**, *7* (17), 7832−7833.

(12) Li, R. N.; Chen, F.; Lam, C. H.; Tsui, O. K. C. Viscosity of PMMA on Silica: Epitome of Systems with Strong Polymer−Substrate Interactions. *Macromolecules* **2013**, *46* (19), 7889−7893.

(13) Chen, F.; Peng, D.; Lam, C. H.; Tsui, O. K. C. Viscosity and Surface-Promoted Slippage of Thin Polymer Films Supported by a Solid Substrate. *Macromolecules* **2015**, *48* (14), 5034−5039.

(14) Stafford, C. M.; Vogt, B. D.; Harrison, C.; Julthongpiput, D.; Huang, R. Elastic Moduli of Ultrathin Amorphous Polymer Films. *Macromolecules* **2006**, *39* (15), 5095−5099.

(15) Torres, J. M.; Stafford, C. M.; Vogt, B. D. Elastic Modulus of Amorphous Polymer Thin Films: Relationship to the Glass Transition Temperature. *ACS Nano* **2009**, *3* (9), 2677−2685.

(16) Evans, C. M.; Narayanan, S.; Jiang, Z.; Torkelson, J. M. Modulus, Confinement, and Temperature Effects on Surface Capillary Wave Dynamics in Bilayer Polymer Films near the Glass Transition. *Phys. Rev. Lett.* **2012**, *109* (3), 038302.

(17) Frank, B.; Gast, A. P.; Russell, T. P.; Brown, H. R.; Hawker, C. J. Polymer Mobility in Thin Films. *Macromolecules* **1996**, *29* (20), 6531−6534.

DOI: 10.1021/acs.macromol.8b00475
Macromolecules XXXX, XXX, XXX−XXX

(18) Zheng, X.; Rafailovich, M.; Sokolov, J.; Strzhemechny, Y.; Schwarz, S.; Sauer, B.; Rubinstein, M. Long-Range Effects on Polymer Diffusion Induced by a Bounding Interface. *Phys. Rev. Lett.* **1997**, *79* (2), 241−244.
(19) Sussman, D. M.; Tung, W. S.; Winey, K. I.; Schweizer, K. S.; Riggleman, R. A. Entanglement Reduction and Anisotropic Chain and Primitive Path Conformations in Polymer Melts under Thin Film and Cylindrical Confinement. *Macromolecules* **2014**, *47* (18), 6462−6472.
(20) Roth, C. B.; Dutcher, J. R. *Mobility on Different Length Scales in Thin Polymer Films*; Marcel Dekker: 2005; pp 1−38.
(21) Tanaka, K.; Taura, A.; Ge, S. R.; Takahara, A.; Kajiyama, T. Molecular Weight Dependence of Surface Dynamic Viscoelastic Properties for the Monodisperse Polystyrene Film. *Macromolecules* **1996**, *29* (8), 3040−3042.
(22) Ellison, C. J.; Torkelson, J. M. The Distribution of Glass-Transition Temperatures in Nanoscopically Confined Glass Formers. *Nat. Mater.* **2003**, *2* (10), 695−700.
(23) Sharp, J.; Forrest, J. Free Surfaces Cause Reductions in the Glass Transition Temperature of Thin Polystyrene Films. *Phys. Rev. Lett.* **2003**, *91* (23), 235701.
(24) Ediger, M. D.; Forrest, J. A. Dynamics near Free Surfaces and the Glass Transition in Thin Polymer Films: A View to the Future. *Macromolecules* **2014**, *47* (2), 471−478.
(25) Priestley, R. D.; Cangialosi, D.; Napolitano, S. On the Equivalence between the Thermodynamic and Dynamic Measurements of the Glass Transition in Confined Polymers. *J. Non-Cryst. Solids* **2015**, *407*, 288−295.
(26) Tung, W. S.; Composto, R. J.; Riggleman, R. A.; Winey, K. I. Local Polymer Dynamics and Diffusion in Cylindrical Nanoconfinement. *Macromolecules* **2015**, *48* (7), 2324−2332.
(27) Williams, M. L.; Landel, R. F.; Ferry, J. D. The Temperature Dependence of Relaxation Mechanisms in Amorphous Polymers and Other Glass-forming Liquids. *J. Am. Chem. Soc.* **1955**, *77* (14), 3701−3707.
(28) Urakawa, O.; Swallen, S. F.; Ediger, M. D.; von Meerwall, E. D. Self-Diffusion and Viscosity of Low Molecular Weight Polystyrene over a Wide Temperature Range. *Macromolecules* **2004**, *37* (4), 1558−1564.
(29) Mansfield, K. F.; Theodorou, D. N. Interfacial Structure and Dynamics of Macromolecular Liquids - a Monte-Carlo Simulation Approach. *Macromolecules* **1989**, *22* (7), 3143−3152.
(30) Rouse, P. E. A Theory of the Linear Viscoelastic Properties of Dilute Solutions of Coiling Polymers. *J. Chem. Phys.* **1953**, *21* (7), 1272.
(31) Doi, M.; Edwards, S. F. *The Theory of Polymer Dynamics*; Clarendon Press: Oxford, 1988.
(32) Ediger, M. D. Spatially Heterogeneous Dynamics in Supercooled Liquids. *Annu. Rev. Phys. Chem.* **2000**, *51* (1), 99−128.
(33) Schmidt-Rohr, K.; Spiess, H. W. Nature of Nonexponential Loss of Correlation above the Glass Transition Investigated by Multidimensional NMR. *Phys. Rev. Lett.* **1991**, *66* (23), 3020−3023.
(34) Cicerone, M. T.; Blackburn, F. R.; Ediger, M. D. Anomalous Diffusion of Probe Molecules in Polystyrene: Evidence for Spatially Heterogeneous Segmental Dynamics. *Macromolecules* **1995**, *28* (24), 8224−8232.
(35) Cicerone, M. T.; Blackburn, F. R.; Ediger, M. D. How Do Molecules Move Near Tg? Molecular Rotation of Six Probes in O-terphenyl across 14 Decades in Time. *J. Chem. Phys.* **1995**, *102* (1), 471−479.
(36) Berthier, L.; Biroli, G.; Bouchaud, J.-P.; Cipelletti, L.; Masri, D. E.; L'Hôte, D.; Ladieu, F.; Pierno, M. Direct Experimental Evidence of a Growing Length Scale Accompanying the Glass Transition. *Science* **2005**, *310* (5755), 1797−1800.
(37) Schiener, B.; Chamberlin, R. V.; Diezemann, G.; Böhmer, R. Nonresonant Dielectric Hole Burning Spectroscopy of Supercooled Liquids. *J. Chem. Phys.* **1997**, *107* (19), 7746−7761.
(38) Reiter, G. Mobility of Polymers in Films Thinner than Their Unperturbed Size. *EPL* **1993**, *23* (8), 579.
(39) Zhang, W.; Yu, L. Surface Diffusion of Polymer Glasses. *Macromolecules* **2016**, *49* (2), 731−735.
(40) Karapanagiotis, I.; Gerberich, W. W. Surface Diffusivity of Thin Polymer Films Measured by a Curvature Driven Flow and Rouse Dynamics. *Surf. Sci.* **2006**, *600* (5), 1178−1184.
(41) Geng, K.; Katsumata, R.; Yu, X.; Ha, H.; Dulaney, A. R.; Ellison, C. J.; Tsui, O. K. C. Conflicting Confinement Effects on the Tg, Diffusivity, and Effective Viscosity of Polymer Films: A Case Study with Poly(isobutyl methacrylate) on Silica and Possible Resolution. *Macromolecules* **2017**, *50* (2), 609−617.
(42) Zhang, Y.; Fakhraai, Z. Decoupling of Surface Diffusion and Relaxation Dynamics of Molecular Glasses. *Proc. Natl. Acad. Sci. U. S. A.* **2017**, *114* (19), 4915−4919.
(43) Chowdhury, M.; Priestley, R. D. Discrete Mobility on the Surface of Glasses. *Proc. Natl. Acad. Sci. U. S. A.* **2017**, *114* (19), 4854−4856.
(44) Tsui, O. K. C.; Russell, T. P.; Hawker, C. J. Effect of Interfacial Interactions on the Glass Transition of Polymer Thin Films. *Macromolecules* **2001**, *34* (16), 5535−5539.
(45) Lang, R. J.; Merling, W. L.; Simmons, D. S. Combined Dependence of Nanoconfined Tg on Interfacial Energy and Softness of Confinement. *ACS Macro Lett.* **2014**, *3*, 758−762.
(46) Reid, D. K.; Alves Freire, M.; Yao, H.; Sue, H.; Lutkenhaus, J. L. The Effect of Surface Chemistry on the Glass Transition of Polycarbonate Inside Cylindrical Nanopores. *ACS Macro Lett.* **2015**, *4* (2), 151−154.
(47) Ye, C. H.; Wiener, C. G.; Tyagi, M.; Uhrig, D.; Orski, S. V.; Soles, C. L.; Vogt, B. D.; Simmons, D. S. Understanding the Decreased Segmental Dynamics of Supported Thin Polymer Films Reported by Incoherent Neutron Scattering. *Macromolecules* **2015**, *48* (3), 801−808.
(48) Napolitano, S.; Glynos, E.; Tito, N. B. Glass Transition of Polymers in Bulk, Confined Geometries, and Near Interfaces. *Rep. Prog. Phys.* **2017**, *80* (3), 036602.
(49) Simmons, D. S. An Emerging Unified View of Dynamic Interphases in Polymers. *Macromol. Chem. Phys.* **2016**, *217* (2), 137−148.
(50) Torres, J. A.; Nealey, P. F.; de Pablo, J. J. Molecular Simulation of Ultrathin Polymeric Films near the Glass Transition. *Phys. Rev. Lett.* **2000**, *85* (15), 3221−3224.
(51) Varnik, F.; Baschnagel, J.; Binder, K. Reduction of the Glass Transition Temperature in Polymer Films: A Molecular-Dynamics Study. *Phys. Rev. E: Stat. Phys., Plasmas, Fluids, Relat. Interdiscip. Top.* **2002**, *65* (2), 021507.
(52) Ngai, K. L. Mobility in Thin Polymer Films Ranging from Local Segmental Motion, Rouse Modes to Whole Chain Motion: a Coupling Model Consideration. *Eur. Phys. J. E: Soft Matter Biol. Phys.* **2002**, *8* (2), 225−235.
(53) Capaccioli, S.; Ngai, K. L.; Paluch, M.; Prevosto, D. Mechanism of Fast Surface Self-Diffusion of an Organic Glass. *Phys. Rev. E* **2012**, *86* (5), 051503.
(54) Tito, N. B.; Milner, S. T.; Lipson, J. E. G. Enhanced Diffusion and Mobile Fronts in a Simple Lattice Model of Glass-Forming Liquids. *Soft Matter* **2015**, *11* (39), 7792−7801.
(55) Lang, R. J.; Simmons, D. S. Interfacial Dynamic Length Scales in the Glass Transition of a Model Freestanding Polymer Film and Their Connection to Cooperative Motion. *Macromolecules* **2013**, *46* (24), 9818−9825.
(56) Starr, F. W.; Douglas, J. F.; Sastry, S. The Relationship of Dynamical Heterogeneity to the Adam-Gibbs and Random First-Order Transition Theories of Glass Formation. *J. Chem. Phys.* **2013**, *138* (12), 12A541.
(57) Napolitano, S.; Cangialosi, D. Interfacial Free Volume and Vitrification: Reduction in Tg in Proximity of an Adsorbing Interface Explained by the Free Volume Holes Diffusion Model. *Macromolecules* **2013**, *46* (19), 8051−8053.
(58) Si, L.; Massa, M. V.; Dalnoki-Veress, K.; Brown, H. R.; Jones, R. L. Chain Entanglement in Thin Freestanding Polymer Films. *Phys. Rev. Lett.* **2005**, *94* (12), 1−4.

DOI: 10.1021/acs.macromol.8b00475
Macromolecules XXXX, XXX, XXX−XXX

(59) Ata, S.; Muramatsu, M.; Takeda, J.; Ohdaira, T.; Suzuki, R.; Ito, K.; Kobayashi, Y.; Ougizawa, T. Free Volume Behavior in Spincast Thin Film of Polystyrene by Energy Variable Positron Annihilation Lifetime Spectroscopy. *Polymer* **2009**, *50* (14), 3343−3346.
(60) Bicerano, J. *Prediction of Polymer Properties*; CRC Press: New York, 2002.
(61) Katzenstein, J. M.; Janes, D. W.; Hocker, H. E.; Chandler, J. K.; Ellison, C. J. Nanoconfined Self-Diffusion of Poly(isobutyl methacrylate) in Films with a Thickness-Independent Glass Transition. *Macromolecules* **2012**, *45* (3), 1544−1552.
(62) McCafferty, E.; Wightman, J. P. Determination of the Concentration of Surface Hydroxyl Groups on Metal Oxide Films by a Quantitative XPS Method. *Surf. Interface Anal.* **1998**, *26* (8), 549−564.
(63) Lakowicz, J. R.; Weber, G. Quenching of Fluorescence by Oxygen. A Probe for Structural Fluctuations in Macromolecules. *Biochemistry* **1973**, *12* (21), 4161−4170.
(64) Priestley, R. D.; Mundra, M. K.; Barnett, N. J.; Broadbelt, L. J.; Torkelson, J. M. Effects of Nanoscale Confinement and Interfaces on the Glass Transition Temperatures of a Series of Poly(n-methacrylate) Films. *Aust. J. Chem.* **2007**, *60* (10), 765−771.
(65) See the Supporting Information. Differential scanning calorimetry confirmed that a PiBMA/PCHE mixture exhibits two different T_g's after annealing at 200 °C for 20 min.
(66) Jin, K.; Torkelson, J. M. Enhanced Tg-Confinement Effect in Cross-Linked Polystyrene Compared to Its Linear Precursor: Roles of Fragility and Chain Architecture. *Macromolecules* **2016**, *49* (14), 5092−5103.
(67) Robeson, J. L.; Tilton, R. D. Effect of Concentration Quenching on Fluorescence Recovery after Photobleaching Measurements. *Biophys. J.* **1995**, *68* (May), 2145−2155.
(68) Davoust, J.; Devaux, P. F.; Leger, L. Fringe Pattern Photobleaching, a New Method for the Measurement of Transport Coefficients of Biological Macromolecules. *EMBO J.* **1982**, *1* (10), 1233−1238.
(69) Sokolov, A. P.; Schweizer, K. S. Resolving the Mystery of the Chain Friction Mechanism in Polymer Liquids. *Phys. Rev. Lett.* **2009**, *102* (24), 248301.
(70) Lange, F.; Judeinstein, P.; Franz, C.; Hartmann-Azanza, B.; Ok, S.; Steinhart, M.; Saalwächter, K. Large-Scale Diffusion of Entangled Polymers along Nanochannels. *ACS Macro Lett.* **2015**, *4* (5), 561−565.
(71) Koga, T.; Li, C.; Endoh, M. K.; Koo, J.; Rafailovich, M.; Narayanan, S.; Lee, D. R.; Lurio, L. B.; Sinha, S. K. Reduced Viscosity of the Free Surface in Entangled Polymer Melt Films. *Phys. Rev. Lett.* **2010**, *104* (6), 066101.
(72) Zhu, L.; Brian, C. W.; Swallen, S. F.; Straus, P. T.; Ediger, M. D.; Yu, L. Surface Self-Diffusion of an Organic Glass. *Phys. Rev. Lett.* **2011**, *106* (25), 256103.
(73) Brian, C. W.; Yu, L. Surface Self-Diffusion of Organic Glasses. *J. Phys. Chem. A* **2013**, *117* (50), 13303−13309.
(74) Mangalara, J. H.; Mackura, M. E.; Marvin, M. D.; Simmons, D. S. The Relationship between Dynamic and Pseudo-Thermodynamic Measures of the Glass Transition Temperature in Nanostructured Materials. *J. Chem. Phys.* **2017**, *146* (20), 203316.
(75) Tung, W. S.; Clarke, N.; Composto, R. J.; Winey, K. I. Temperature Dependence of Polymer Diffusion in MWCNT/PS Nanocomposites. *Macromolecules* **2013**, *46* (6), 2317−2322.

DOI: 10.1021/acs.macromol.8b00475
Macromolecules XXXX, XXX, XXX−XXX